SEISMICA

Microseismicity at the Time of a Large Creep Event on the Calaveras Fault is Unresponsive to Stress Changes

L. Huang ⓘD * [1], **S. Schwartz** ⓘD [1], **E.E. Brodsky** ⓘD [1]

[1]Department of Earth and Planetary Sciences, University of California, Santa Cruz, United States

Abstract   The potential relationship between surface creep and deeper geological processes is unclear, even on one of the world's best-studied faults. From June to August 2021, a large creep event with surface slip of more than 16 mm was recorded on the Calaveras fault in California, part of the San Andreas fault system. This exceptionally well-instrumented event provides an excellent opportunity to investigate the relationship between earthquakes and large surface creep. We therefore tripled the number of earthquakes in the Northern California Earthquake Catalog in the region of the creep event for all of 2021. This was accomplished by implementing earthquake detection techniques based on both template matching (EQCorrscan) and AI-based automatic earthquake phase picking (PhaseNet). After manual inspection, the detected earthquakes were first located using Hypoinverse and subsequently relocated via GrowClust. Our enhanced catalog indicates that the spatiotemporal pattern of earthquakes here is not strongly influenced by the creep event and is better explained by structural heterogeneity than transient stress changes, indicating a decoupling of seismicity and surficial creep on this major fault.

Non-technical summary   Creep events are episodes of accelerated aseismic slip observed on the surface of faults and their connection to deeper fault segments remains unknown. Our study focuses on one of the most significant creep events on the Calaveras Fault, with a surface displacement exceeding 16 mm. We aim to explore whether or not there is interaction between surface creep and deep earthquake activity. We improve the earthquake catalog during the creep event by applying AI-based detector and template matching techniques to find additional small earthquakes, not reported in the standard Northern California Earthquake catalog. We locate these new events and relocate all seismicity using a consistent velocity model and location algorithm. Our results show that initially observed earthquake migration during the creep event is not distinguishable from prior earthquake patterns, and thus it is not convincing that the migration reflects the propagation of deep slipping patches. The earthquake activity is similar to the historic distribution of earthquakes, which has a persistent gap in seismicity along the fault. This suggests that structural heterogeneity may be a prevailing factor controlling seismicity.

1 Introduction

The Calaveras fault segment between Gilroy and Hollister (Figure 1) is capable of generating both earthquakes and aseismic slip. This segment experiences earthquakes with a range of magnitudes from micro to moderate ($1 < M < 4$) at depths between primarily 2 and 10 km, indicating that the fault is not entirely locked (Schaff et al., 2002). Additionally, both steady creep and accelerated aseismic slip episodes have been observed on the fault surface here (Evans et al., 1981; Schulz et al., 1982). This segment of the Calaveras fault is also conspicuous for being at the transition between locked to the north and creeping to the south (Oppenheimer et al., 1990). Thus, it is an excellent place to study the interactions and relationships between creep events and earthquakes.

Creep events on the Calaveras have been observed at multiple locations since the 1960s (Schulz, 1989). The U.S. Geological Survey creepmeter station XSH1 recorded one of the most significant recent Calaveras creep events between June and August 2021 with a total slip of 16 mm occurring over two separate transient episodes. Although XSH1 has intermittent historical records, this instrument has detected at least six creep events larger than 10 mm since 1974 (Figure S1; Historic creep events recorded by creepmeters XSH1, HLC1, and HLD1). Notably, the 2021 event is larger than most of the historic creep transients recorded at this station. Creep events on other faults are typically smaller than 20 mm (Gittins and Hawthorne, 2022). The plate velocity at this site is approximately 15 mm per year (Chaussard et al., 2015; Li et al., 2023; Schulz et al., 1982), so this specific creep event accounted for the slip deficit accumulated over approximately one year.

Creep events recorded on surface creepmeters are generally thought to be shallow surface movements,

---

yet determining their depth extent remains challenging. Some studies investigating creep events on the Calaveras Fault, including creepmeter and strainmeter observations and accompanying kinematic modeling, suggest at least some creep events are shallow (Evans et al., 1981; King, 2019; Slater and Burford, 1979). Evans et al. (1981) utilized near-field strain data to examine the depth extent of two creep events on this same Calaveras fault segment in 1977. Their analysis showed that one of the creep events with 9 mm of surface displacement had a horizontal extent of between 6.6 and 8.4 kilometers and did not extend deeper than 500-1400 meters. Gittins and Hawthorne (2022) conducted a detailed investigation of creep events on the creeping section of the San Andreas Fault with a range of magnitudes. They found that some creep events are isolated, being recorded at only one or two stations, while others extend more than 10 km and possibly up to 31 km and are detected at multiple creepmeters. The largest creep events sometimes skip intermediate surface creepmeters, implying that the slip is continuous at depth while segmented on the surface. A study focused on the North Anatolian Fault combining creepmeter data and shear strain rates indicated that the depth of creep events extended to 3-7 km (Bilham et al., 2016). Furthermore, standard elastic theory would suggest that the depth of creep events is comparable to their horizontal extent, implying that the large creep events with significant horizontal extent are likely to extend into the seismogenic zones (Segall, 2010). If we assume a ratio of slip to length similar to that of the Evans et al. (1981) event, the 2021 creep event, which is characterized by a slip displacement of 16 mm, may have occurred over a patch exceeding 12 kilometers in horizontal extent, with potentially commensurate effects at depth.

The triggering relationship between earthquakes and creep events also motivates further study. Previous research has reported surface creep triggered by local and remote earthquakes (Allen et al., 1972; Bilham and Castillo, 2020; Hirao et al., 2021; Tymofyeyeva et al., 2019; Victor et al., 2018), in some cases with aseismic slip propagating days after the earthquake (Bilham and Castillo, 2020). There are also observations of earthquakes preceded by creep events or shallow aseismic slip (Heimpel and Malin, 1998; Linde et al., 1988; Thurber, 1996; Thurber and Sessions, 1998).

By examining the Northern California Earthquake Data Center (NCEDC) catalog (NCEDC, 2014) (Figure 2), Bilham et al. (2021) suggested a potential southeastward migration of microseismic clusters during a time period spanning March to August 2021, associated with the 2021 Calaveras creep event. Concurrently, they observed an increase in Radon and CO_2 gas emissions detected at a proximal borehole. This postulated earthquake migration pattern initiated approximately 10 km north of the creepmeter station XSH1 in March and was characterized by an increase in earthquake activity. Following a hiatus in seismicity, earthquake activity increased southward, locating directly beneath the creepmeter in June and coincident with the onset of accelerated surface slip. Seismicity then moved farther s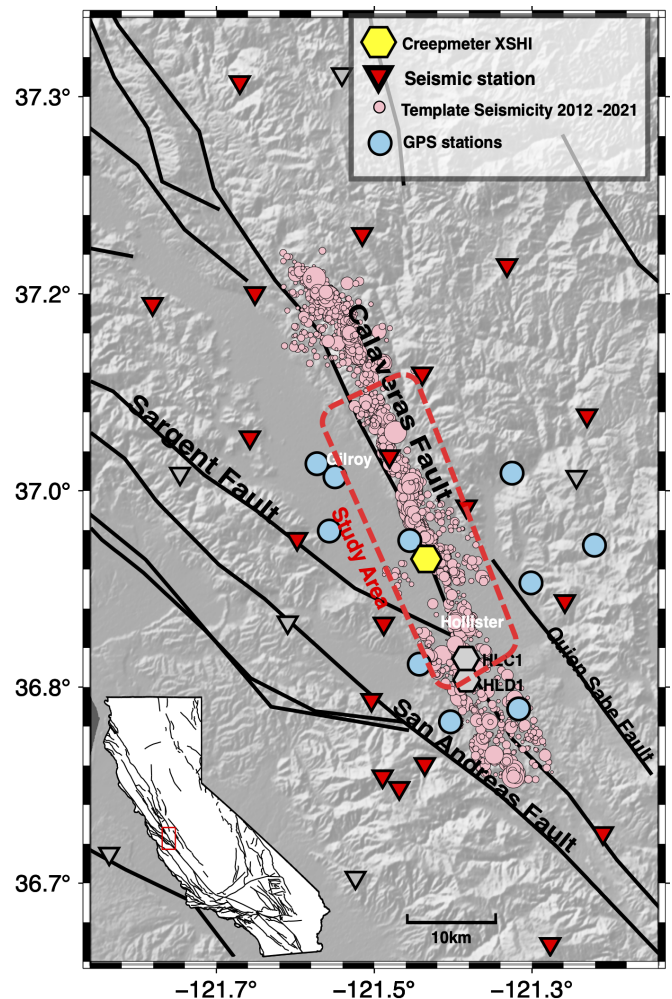outh, culminating in a notable earthquake cluster in July/August that coincided with the largest surface displacement; however, by this time the seismic activity had already moved past the creepmeter to the south (Figure 2). The lag between aseismic slip at depth, implied by the earthquake migration pattern, and the slip at the surface offers a promising way to improve our understanding of the propagation of aseismic slip, the relationship between propagating slip episodes and microseismicity, and the horizontal and vertical extent of the creep event.

In this study, we aim to expand the catalog of recorded earthquakes in the region of the 2021 creep event for all of 2021 and explore the temporal and spatial pattern of the microseismicity to elucidate the relationship between earthquakes, surface creep, and potential aseismic slip at seismogenic depths.

Figure 1 Map of the study region and instruments. Northern California Seismic Network (NCSN) seismic stations are shown as red (used) and transparent (unused) triangles. GPS stations are shown as blue circles. Creepmeters are indicated with the hexagons with only XSH1 operating during the 2021 creep event. Template earthquakes from the Double Difference Real Time (DDRT) Catalog between 2012-2021 are shown as pink circles, sized by magnitude. Faults plotted are from the USGS Quaternary Faults and Folds database (https://www.usgs.gov/natural-hazards/earthquake-hazards/faults). Inset map of California shows the location of the study region as a red box.
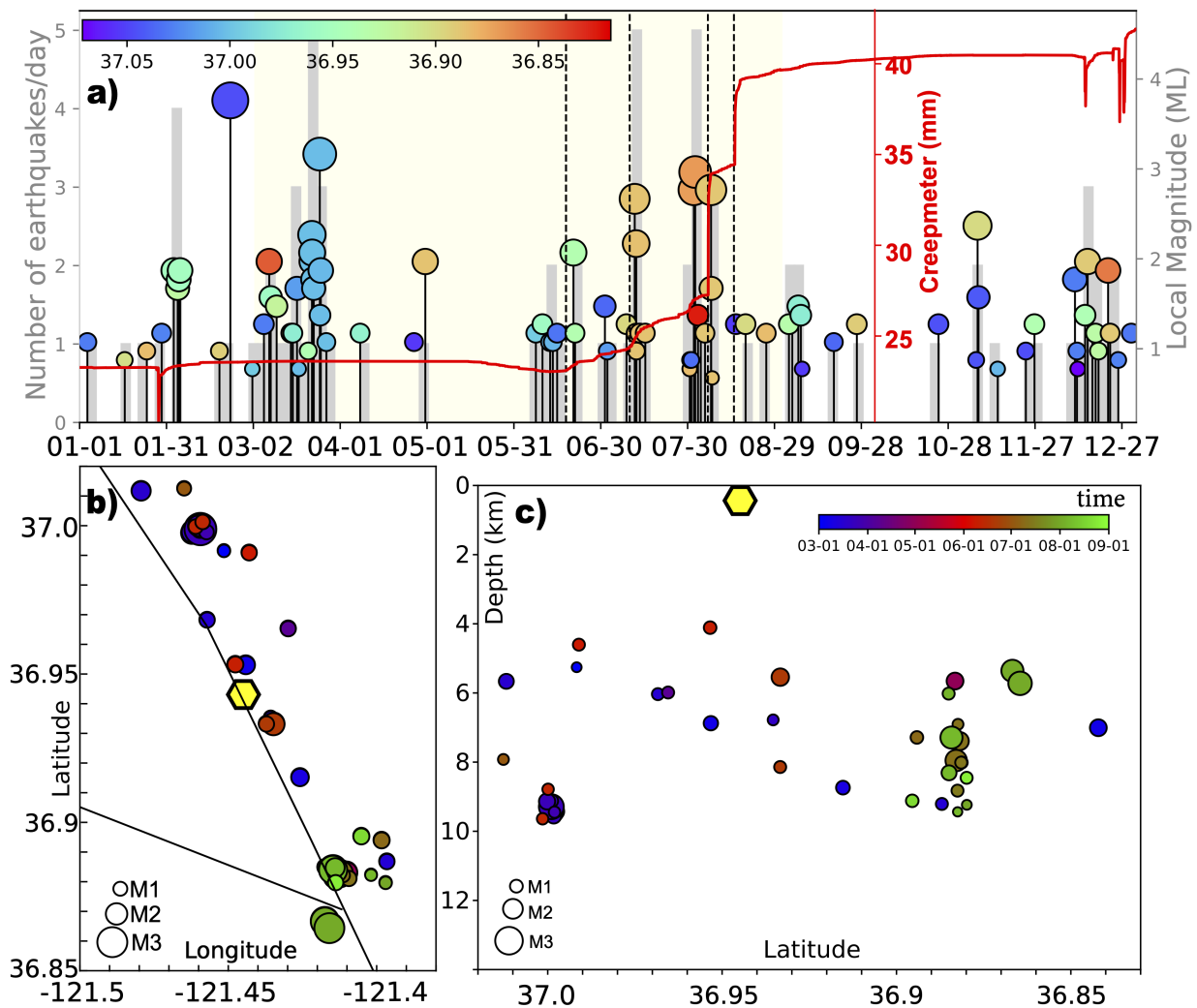
Figure 2 NCEDC Seismicity and Creep Data Correlation on the Calaveras Fault in 2021. (a) Left y-axis: histogram of seismic events (gray bars); right y-axis: earthquake magnitude (circles), and continuous displacement measured by creepmeter XSH1 (red line). The earthquake circles are sized by magnitude and colored by latitude. Yellow bar highlights the time window from March 1st to September 1st. Black vertical dashed lines mark the dates of aseismic transients. (b & c) Map view (b) and profile (c) of seismic activity recorded between March and August 2021. Earthquakes are sized by magnitude and colored by time. The yellow hexagon represents creepmeter station XSH1.

2 Data and Methods

Our processing procedure includes P and S wave phase detection and association using various methods, earthquake location, relocation, and local magnitude calculation for events occurring in 2021 over a relatively large region surrounding the 2021 Calaveras creep event. Many of the events detected and located occur outside our primary region of interest, as indicated by the dashed red box in Figure 1. To maintain the consistency and completeness of the catalog, we focus only on the events located in the area of interest. This workflow allows us to build a comprehensive catalog for the study area without overlooking any significant, detectable events.

2.1 Seismic Data

We have chosen 21 seismic stations (Figure 1) from the Northern California Seismic Network (NCSN) strategically located around the area of interest, all of which

have been in continuous operation from 2012 to 2022. The 21 seismic stations used for this study include a variety of instruments: some stations have broadband seismometers, others have accelerometers, and some are equipped with short-period seismometers. The specific type of instrument at each station varies based on waveform availability.

2.2 Earthquake Detection

To maximize the detection of seismic body wave arrivals, we employ a dual approach: We utilize a deep neural network-based earthquake phase picker, PhaseNet (Zhu and Beroza, 2019), and perform template matching via EQcorrscan (Chamberlain et al., 2017). Trained on over 600,000 waveforms from the NCEDC which encompasses our area of interest, PhaseNet offers reliable performance. The method can detect P and S arrivals on single-station waveforms and estimate the probability of each pick. In this study, PhaseNet facilitated the detection of 1,099,601 P arrivals and 1,291,841

S arrivals with a confidence level exceeding 0.3 in the year 2021. Although most of these arrivals are unassociated or pertain to earthquakes outside the research area, they have been instrumental in identifying numerous new seismic events.

EQcorrscan specializes in recognizing body wave arrivals for repeating and near-repeating earthquakes that have highly correlated waveforms with template events. For this analysis, we drew upon 1,893 earthquakes from the Real-Time Double-Difference Catalog (DDRT) spanning 2012 to 2021 as template events, plotted as pink dots in Figure 1 (Waldhauser and Schaff, 2008; Schaff and Waldhauser, 2005). During 2021, there were 5413 picks detected as matched events with a cross-correlation coefficient higher than 0.6 for at least four stations. After removing the picks that were repeated matches or detected by PhaseNet and the NCEDC catalog, this strategy enabled the identification of 345 new P arrivals, with S arrivals being identified manually.

Following a careful manual inspection of the quality of the obtained picks, we apply the rapid association algorithm REAL (Zhang et al., 2019) to associate them. This algorithm conducts a grid search in the vicinity of the closest station, counting the number of picks that fall within the arrival time residual threshold for each grid cell. It then identifies the grid cell with the optimal convergence of the highest number of picks and the smallest average arrival time discrepancy as the source location. In this study, we limit our associations to events with a minimum of 4 P arrivals and 5 total arrivals and which have a residual arrival time under 0.6 seconds. The grid utilized for the search measured 0.2° and 2 km in horizontal and vertical spacing. As a result of this process, 3527 events were generated during 2021.

2.3 Location and Relocation

We employ the HYPOINVERSE program (Klein) to determine earthquake locations. Through extensive testing of various earthquake location programs, we have found that the accuracy of earthquake locations, particularly for smaller events with fewer picks, is highly dependent on both the location method and the velocity model employed. Since we want to jointly relocate historical events from the NCEDC catalog, we opted for the HYPOINVERSE program in alignment with their practices. This approach ensures consistency as we also adopt the same station corrections and velocity models used in the NCEDC catalog. Details regarding the velocity model, error analysis of the locations, and error comparison with the NCEDC catalog are included in the supplementary materials.

Next, we utilize the GrowClust program to facilitate relocation (Trugman and Shearer, 2017). GrowClust stands out for its high computational efficiency as a relative earthquake relocation algorithm. Initially, it establishes the cluster relationships between event pairs based on the cross-correlation coefficient of waveforms at identical stations and the distance between original locations. Subsequently, it relocates the clustered events employing a grid-search algorithm to a new location that minimizes the differential arrival time resid-

ual between the event pairs. In this procedure, we incorporated 1,893 events from the Real-Time Double-Difference Catalog (DDRT) to ensure a substantial number of events were both clustered and relocated. With a correlation coefficient threshold of 0.9, this approach resulted in the relocation of 2002 events out of a total of 3326 in the year 2021.

2.4 Local Magnitude

We computed the local magnitude for all earthquakes recorded in 2021, incorporating events from the NCEDC catalog to maintain consistency, as prescribed by methods detailed in Gutenberg and Richter (1956) and Bakun and Joyner (1984). For each event, we determined the maximum half peak-to-peak amplitude A(mm) within a time window that encompasses both P and S arrivals. The local magnitude was then calculated at each station equipped with two horizontal channels, utilizing the following equation (Bakun and Joyner, 1984):

$$M_L = log_{10}A + log_{10}D + 0.0031D + 0.7 \qquad (1)$$

Here, D represents the distance between the hypocenter and the station. We established the final magnitude value by calculating the mean of the magnitude measurements obtained across all available stations. Through this method, we derived the local magnitudes (M_L) for 3326 earthquakes in 2021.

3 Results

By integrating multiple detection techniques with a consistent earthquake location and relocation algorithm, we substantially increased the spatial and temporal resolution of the earthquake activity in the region for the year 2021. In the study area, we increased the number of recorded earthquakes from 85 to 275, revealing many previously undetected small events (Figure 3). Notably, our earthquake magnitude of completeness is 0.5, determined by minimizing the average square error of the fitted Gutenberg-Richter law, with the b-value estimated following Maximum Likelihood Estimation (Aki, 1965). This represents a significant improvement compared to the magnitude of completeness of 1.4 from the NCEDC catalog. The enhanced detection of smaller-magnitude events is crucial for understanding the relationship among earthquakes, creep events, and structural heterogeneity.

Our enhanced catalog shows the same southeastward migration of earthquake clusters as observed in the NCEDC catalog (Compare Figures 2a and 3a). However, contrary to expectations, the newly added events in April and May introduce more variability to the overall migration pattern rather than reinforcing and clarifying its continuous southward propagation. The newly discovered April to May seismicity is located south of the June cluster and therefore interrupts the monotonic southward migration pattern from cluster 1 to cluster 3 (Figure 4c) initially noted by Bilham et al. (2021). The lack of a systematic pattern in seismicity suggests that the earthquake locations are not strongly influenced by the surface creep event.
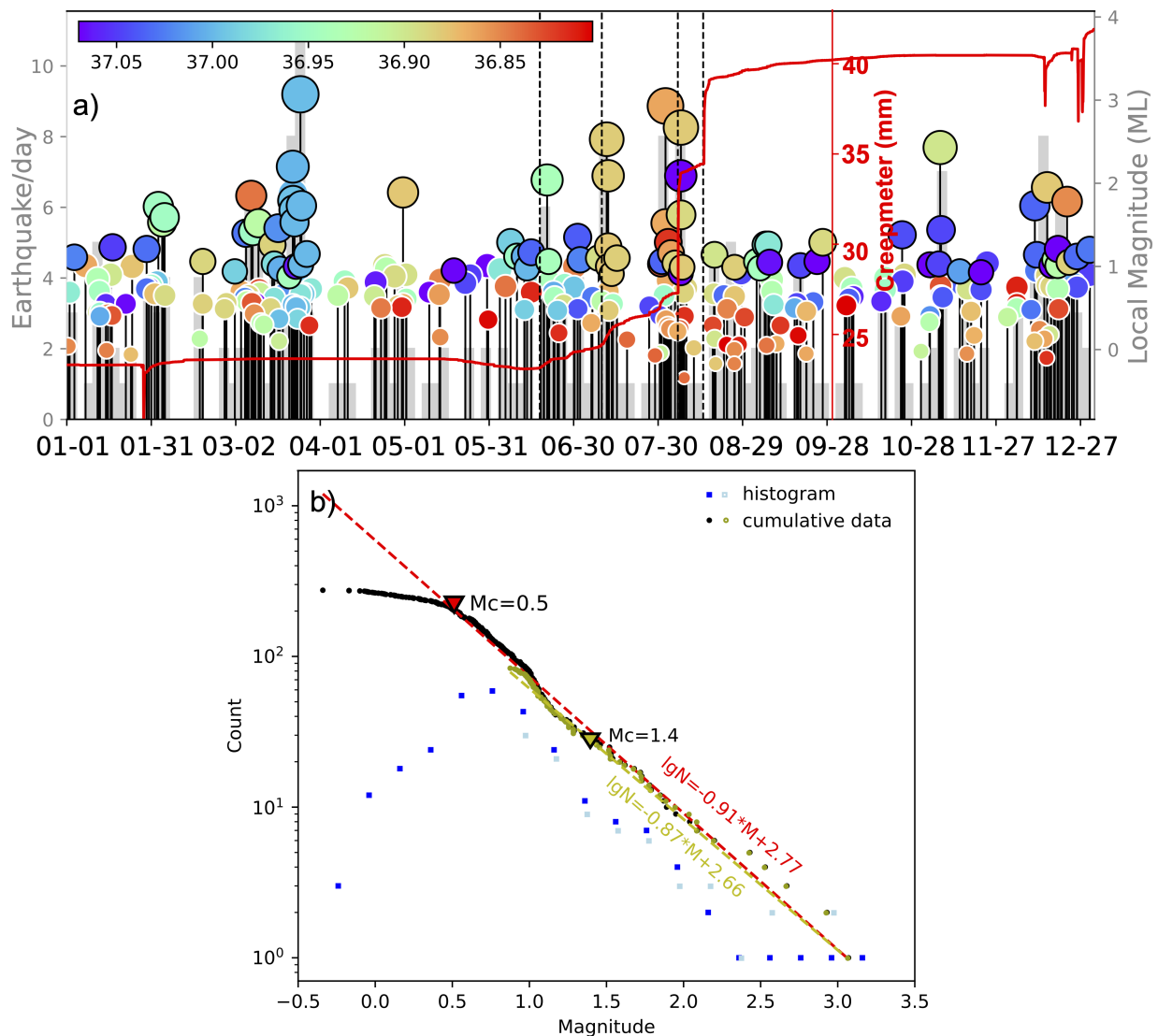
Figure 3 2021 Seismic Catalog Overview. (a) Earthquake Magnitude and Spatial Distribution: The plot shows earthquakes as circles (sized by magnitude and colored by latitude) against a background histogram (gray bars) of seismic event frequency. The continuous displacement recorded at creepmeter XSH1 is depicted as a red line. White-edged circles indicate newly detected seismic events. Black vertical dashed lines mark the dates of aseismic transients. (b) Comparative Magnitude Analysis: This figure displays the magnitude distribution of the produced catalog (blue squares) alongside the network catalog (light blue squares). The Gutenberg-Richter distribution fit for both catalogs is shown, with the produced catalog represented by black dots and a red dashed line, and the NCEDC catalog by green dots and a green dashed line.

The distribution of earthquakes revealed by our enhanced catalog is very similar to the historical seismicity distribution between 2012 and 2020 (represented as grey dots in Figure 4b) from the Double-difference Earthquake Catalog for Northern California and the Real-Time Double Difference catalog (Waldhauser and Schaff, 2008; Schaff and Waldhauser, 2005). A significant 75% of events in our catalog are clustered with the historical events from 2012 to 2020, based on a cross-correlation coefficient criterion of 0.8. Notably, a distinct feature of both seismicity patterns is evident around latitude 36.9° (Figure 5), where historically fewer earthquakes have been recorded and the normalized accumulated seismic moment is substantially lower than in other areas. During the period of one of the largest creep events, and despite lowering the magnitude of completeness and more than tripling the number of earthquakes, there were minimal new detections

in this seismicity gap. This suggests that even if the creep event has some influence on the seismic activity, it does not outweigh the prevailing structural control of seismicity in this region.

4 Discussion

4.1 Distribution of accumulated seismic moment

The distribution of accumulated seismic moment of earthquakes in our catalog along the fault trace is calculated and normalized by time and distance (Figure 5). The along-fault distances of the earthquakes are measured from the northwest point of the reference line in Figure 4a to the projections of the earthquakes on this line, and they are further illustrated in Figure S7 (along-fault distance of earthquakes). We generated
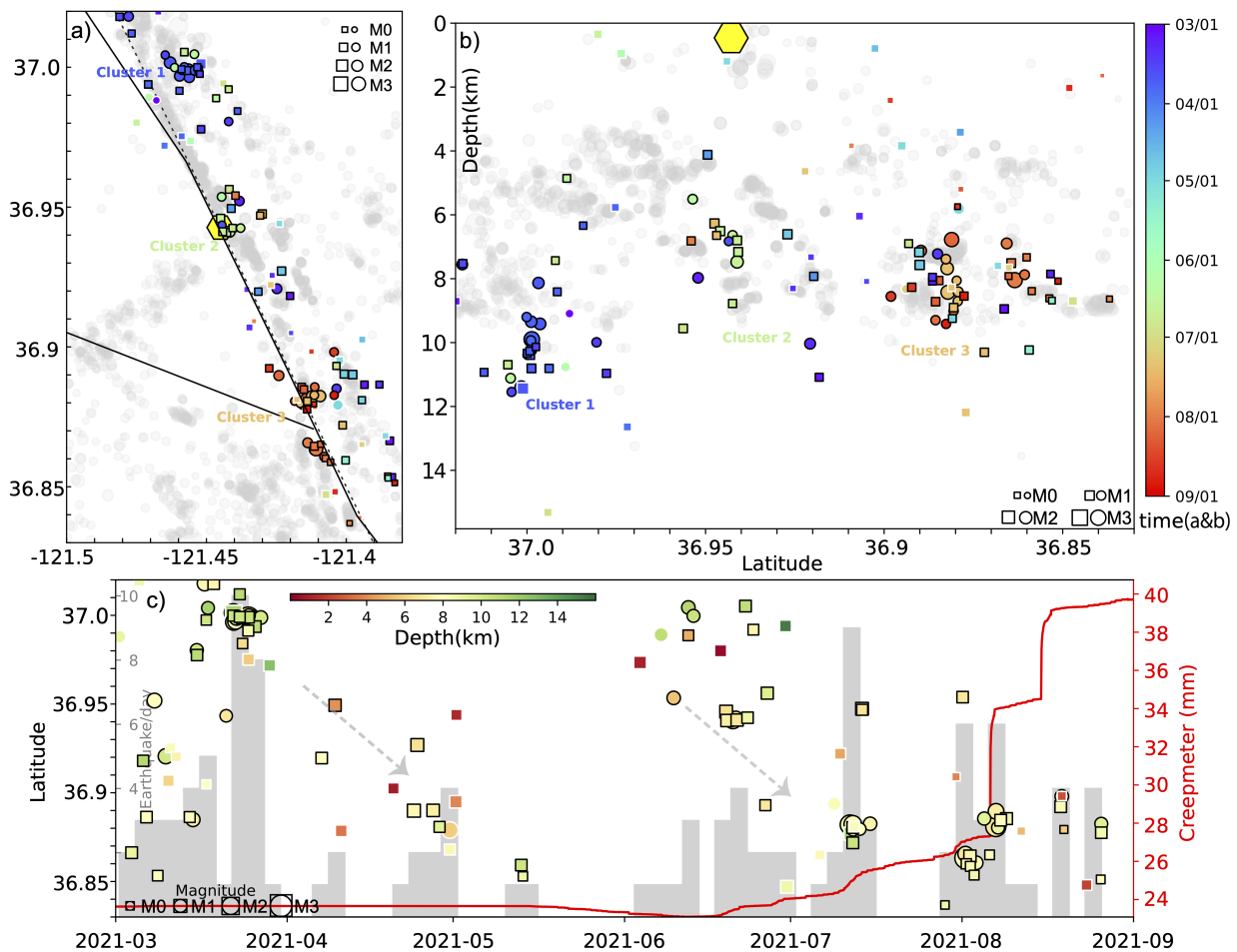
Figure 4 Distribution and Characteristics of Detected Earthquakes (March-August 2021). (a) Map view and (b) cross-sectional profile illustrating the spatial distribution of detected earthquakes, symbolized by circles and squares (newly detected). All detected earthquakes are selected within 1 km on the left side and 3 km on the right side of the Calaveras fault, and they are sized by local magnitude and colored by occurrence time. Circles with black edges indicate earthquakes that were clustered and relocated by GrowClust, and circles with gray edges are earthquakes that were not clustered. Gray dots are earthquakes included in the NCEDC catalog from 2012 to 2020. The yellow hexagon indicates the location of creepmeter XSH1. The gray dashed line in the map view is the reference line for along-fault distances of the earthquakes. (c) Circles and squares (newly detected) show the latitudinal position of earthquakes, with gray bars showing the corresponding earthquake rate. The red line shows the fault surface slip recorded by creepmeter XSH1. For comparison, Figure S4 shows the same data but includes only events above the magnitude of completeness.

moment accumulation plots for two distinct time periods to more clearly illustrate how the smaller events in our expanded earthquake catalog disrupt the monotonic southward migration pattern identified between March and August 2021 in the NCEDC catalog. Both time periods indicated in Figure 5, March 20-May 20 and May 21-September 1, possess an apparent southward migration of seismic moment and are not strongly distinguishable from the background pattern (gray lines in Figure 5, further illustrated in Figure S8). Notably, a gap in seismicity present between 1984 and 2020 around latitude 36.9° persists during the creep event, and demonstrates the prevailing effect of structural heterogeneity on seismic activity since at least 1984. Additionally, the level of seismic activity during this period was not stronger than historical patterns, implying that the seismicity is not sufficiently distinct to robustly indicate an influence by the surface creep, even though the timing appears to align well.

This seismicity gap is approximately 1 km wide along

the Calaveras Fault (Figure 4) and in addition to reduced seismic activity this region also has a lower slip rate compared to adjacent sections of this fault (Li et al., 2023). The lower seismic activity and reduced slip rate strongly suggest that this segment of the fault is locked, implying that a particular characteristic is actively preventing the release of accumulated stress in this area. A plausible explanation involves variations in frictional properties along the fault zone, potentially attributed to differences in lithology (Marone, 1998). Although detailed geological information at depth is unknown, outcrops in the nearby region support lithologic heterogeneity (Wahrhaftig et al., 1993). In particular, an outcrop of older gravels that correlates with the locked area suggests a lithologic and potentially structural heterogeneity that might continue to depth (Dibblee and Minch, 2006). A physically viable hypothesis is that a sliver of rocks with intrinsically higher frictional resistance, such as sandstones, quartzites or unaltered igneous rock, dominates the area impeding slip and thus
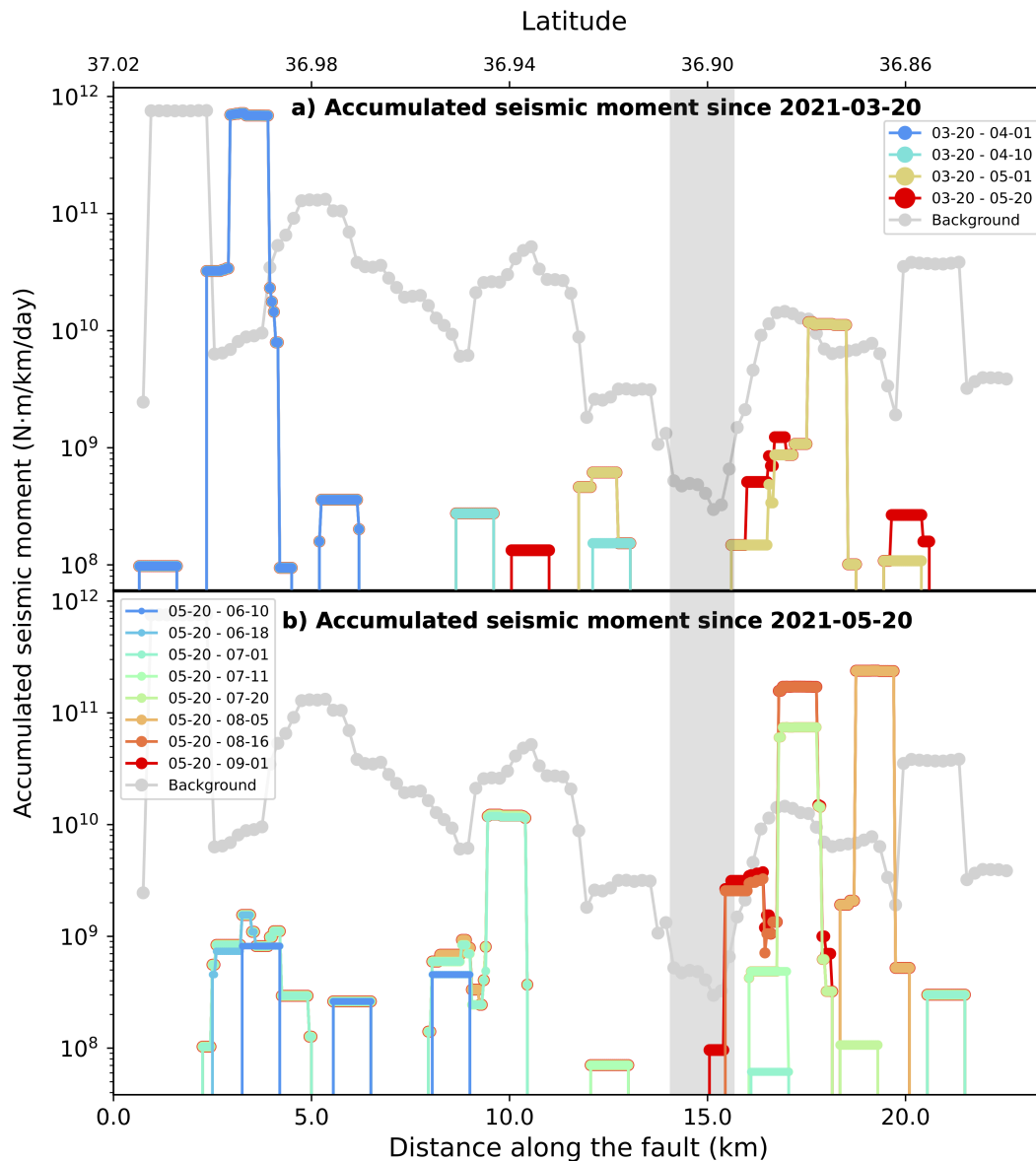
Figure 5 Normalized accumulated seismic moment along the fault in two distinct time periods, 2021-03-20 through 2021-05-20 (upper panel) and 2021-05-21 through 2021-09-01 (lower panel). Colored lines indicate moment accumulation from the starting date in the subtitle to the end date shown by the dots' color. The sizes of dots are slightly different so that the lines would not fully block each other. Gray lines show the normalized accumulated seismic moment of earthquakes from 1984 to 2020. Gray bar marks the seismicity gap. For comparison, Figure S5 shows the same data but includes only events above the magnitude of completeness.

reducing seismic activity. Alternatively, the presence of a significant geometric anomaly, such as a large 'bump' on the fault surface, could increase the frictional resistance, effectively stabilizing this segment of the fault (Eijsink et al., 2022). A third possibility is that hydrogeologic factors could play a role and lower pore pressure here would result in higher effective Coulomb stress. In the absence of direct evidence for any of these three physical possibilities, we favor one of the first two as most plausible given the geometry, compression ridge and known heterogeneity of lithologies rafted along the San Andreas.

4.2 Interpretation of migration

Although we observe increases and decreases of seismic activity at various locations over time that are consistent

with a southeastward migration, the overall pattern is neither continuous along the fault nor monotonic, lacking consistent detail. Furthermore, it is indistinguishable from other regional short-term migrations. For instance, the newly discovered April to May 2021 seismicity located in the most southern section led to a seismicity pattern from March to May with a southward migration, similar to the one from June to August (dashed gray arrows in Figure 4c). Therefore, it would be imprudent to rule out the possibility that these migrations are coincidentally arranged spontaneous seismicity and interpret the migration pattern as indicative of aseismic creep at depth.

4.3 Impact of velocity model on depth determination

The lack of a pattern in the depth distribution of the earthquakes accompanying the surface creep event (Figure 4b) is critical to our interpretation that seismicity appears unresponsive to the 2021 creep event. It is therefore important to access the accuracy of our depth determinations and their dependency on the velocity model. We evaluated earthquake depths determined using Hypoinverse and multiple, region dependent, velocity models adopted by the NCEDC compared with those determined using a single local velocity model (Coyote Lake). Our results demonstrate how the selection of the velocity model significantly affects the depth estimations and can introduce misleading artifacts. For example, the average depth of earthquakes in our 2021 catalog calculated using a single velocity model (Coyote Lake) is 1 km shallower and has a strong southeastward shallowing trend compared to depths determined with multiple velocity models (compare Figures S6a and 6b). This same shallowing trend is evident when we use the Coyote Lake velocity model and NCSN arrival times to locate all events in this region between 2000-2020, but disappears when multiple velocity models are employed (Figure S6c). Our tests on the effect of different velocity models on earthquake depth suggest that apparent depth migrations are not always robust and may be an artifact introduced by the velocity model. It is noteworthy that earthquake depth determinations are generally less reliable than epicentral locations. Therefore, maintaining uniformity in velocity models and location methodology is crucial to compile a new catalog and to compare or integrate it with existing catalogs.

5 Conclusion

We enhanced the earthquake catalog in the study region in 2021 by applying multiple detection methods. We improved the locations, more than tripled the number of earthquakes, and decreased the magnitude of completeness significantly. Our results show that one of the largest surface creep events recorded on the Calaveras Fault, with 16 mm of displacement, does not have obvious manifestations in seismicity. The pattern of the accumulated seismic moment in the study time window is not distinguishable from that of the prior seismicity, which indicates that these earthquakes are not necessarily influenced by the temporal stress change of the surface creep event. The location of all detected earthquakes in 2021 is consistent with the pattern of historical seismicity. The accumulated seismic moment between 2000 and 2020 near latitude 36.9° is significantly lower than other regions of the fault and this seismicity gap is evident during the 2021 creep event. Our results suggest that seismicity here is mainly controlled by persistent structural heterogeneity that has existed since at least 1984.

Data and code availability

Waveform data, metadata, or data products for this study were accessed through the Northern California Earthquake Data Center (NCEDC), doi:10.7932/NCEDC. Fault data are from the USGS Quaternary Faults and Folds database(https://www.usgs.gov/natural-hazards/earthquake-hazards/faults). Creepmeter data can be obtained at the USGS website (https://earthquake.usgs.gov/monitoring/deformation/data/download.php). We used the open-source software PhaseNet (Zhu and Beroza, 2019), EQcorrscan (Chamberlain et al., 2017), REAL (Zhang et al., 2019), HYPOINVERSE (Klein), and Grow-Clust (Trugman and Shearer, 2017) for earthquake detection, association, location, and relocation. The station correction files and velocity models can be found at https://ncedc.org/pub/catalogs/ncsn/hypoinverse/.

Competing interests

The authors declare that they have no conflict of interest.

References

Aki, K. Maximum likelihood estimate of b in the formula log N= a-bM and its confidence limits. *Bull. Earthquake Res. Inst., Tokyo Univ.*, 43:237–239, 1965.

Allen, C. R., Wyss, M., Brune, J. N., Grantz, A., and Wallace, R. E. Displacements on the Imperial, Superstition Hills, and San Andreas faults triggered by the Borrego Mountain earthquake. *US Geol. Surv. Prof. Pap*, 787:87–104, 1972.

Bakun, W. H. and Joyner, W. B. The ML scale in central California. *Bulletin of the Seismological Society of America*, 74(5): 1827–1843, 1984. doi: 10.1785/BSSA0740051827.

Bilham, R. and Castillo, B. The July 2019 Ridgecrest, California, Earthquake Sequence Recorded by Creepmeters: Negligible Epicentral Afterslip and Prolonged Triggered Slip at Teleseismic Distances. *Seismological Research Letters*, 91(2A):707–720, 01 2020. doi: 10.1785/0220190293.

Bilham, R., Ozener, H., Mencin, D., Dogru, A., Ergintav, S., Cakir, Z., Aytun, A., Aktug, B., Yilmaz, O., Johnson, W., and Mattioli, G. Surface creep on the North Anatolian Fault at Ismetpasa, Turkey, 1944–2016. *Journal of Geophysical Research: Solid Earth*, 121(10):7409–7431, 2016. doi: https://doi.org/10.1002/2016JB013394.

Bilham, R., Langbein, J. O., Ericksen, T. L., Nevitt, J. M., Brooks, B. A., and Mencin, D. J. Fault-zone gas venting and aseismic slip: ventilation or lubrication? In *2021 SCEC Annual Meeting*, September 2021.

Chamberlain, C. J., Hopp, C. J., Boese, C. M., Warren-Smith, E., Chambers, D., Chu, S. X., Michailos, K., and Townend, J. EQcorrscan: Repeating and Near-Repeating Earthquake Detection

and Analysis in Python. *Seismological Research Letters*, 89(1): 173–181, 12 2017. doi: 10.1785/0220170151.

Chaussard, E., Bürgmann, R., Fattahi, H., Johnson, C. W., Nadeau, R., Taira, T., and Johanson, I. Interseismic coupling and refined earthquake potential on the Hayward-Calaveras fault zone. *Journal of Geophysical Research: Solid Earth*, 120(12): 8570–8590, 2015. doi: https://doi.org/10.1002/2015JB012230.

Dibblee, T. W. and Minch, J. A. Geologic map of the San Felipe quadrangle, Santa Clara San Benito Counties, California. 1:24,000, 2006. Dibblee Geological Foundation, Dibblee Foundation Map DF-229.

Eijsink, A. M., Kirkpatrick, J. D., Renard, F., and Ikari, M. J. Fault surface morphology as an indicator for earthquake nucleation potential. *Geology*, 50(12):1356–1360, 10 2022. doi: 10.1130/G50258.1.

Evans, K. F., Burford, R. O., and King, G. C. P. Propagating episodic creep and the aseismic slip behavior of the Calaveras Fault north of Hollister, California. *Journal of Geophysical Research: Solid Earth*, 86(B5):3721–3735, 1981. doi: https://doi.org/10.1029/JB086iB05p03721.

Gittins, D. B. and Hawthorne, J. C. Are Creep Events Big? Estimations of Along-Strike Rupture Lengths. *Journal of Geophysical Research: Solid Earth*, 127(1):e2021JB023001, 2022. doi: https://doi.org/10.1029/2021JB023001.

Gutenberg, B. and Richter, C. F. Earthquake magnitude, intensity, energy, and acceleration: (Second paper). *Bulletin of the seismological society of America*, 46(2):105–145, 1956. doi: 10.1785/BSSA0460020105.

Heimpel, M. and Malin, P. Aseismic slip in earthquake nucleation and self-similarity: evidence from Parkfield, California. *Earth and Planetary Science Letters*, 157(3):249–254, 1998. doi: https://doi.org/10.1016/S0012-821X(98)00035-1.

Hirao, B., Savage, H., and Brodsky, E. E. Communication Between the Northern and Southern Central San Andreas Fault via Dynamically Triggered Creep. *Geophysical Research Letters*, 48(13):e2021GL092530, 2021. doi: https://doi.org/10.1029/2021GL092530.

King, C.-Y. Kinematics of Slow-Slip Events. In Santos-Reyes, J., editor, *Earthquakes*, chapter 13. IntechOpen, Rijeka, 2019. doi: 10.5772/intechopen.84904.

Klein, F. User's Guide to HYPOINVERSE-2000, a Fortran Program to Solve for Earthquake Locations and Magnitudes, Version 1.40, June 2014. doi: 10.13140/2.1.4859.3602.

Li, Y., Bürgmann, R., and Taira, T. Spatiotemporal Variations of Surface Deformation, Shallow Creep Rate, and Slip Partitioning Between the San Andreas and Southern Calaveras Fault. *Journal of Geophysical Research: Solid Earth*, 128(1):e2022JB025363, 2023. doi: https://doi.org/10.1029/2022JB025363.

Linde, A. T., Suyehiro, K., Miura, S., Sacks, I. S., and Takagi, A. Episodic aseismic earthquake precursors. *Nature*, 334(6182): 513–515, 1988. doi: https://doi.org/10.1038/334513a0.

Marone, C. Laboratory-derived friction laws and their application to seismic faulting. *Annual Review of Earth and Planetary Sciences*, 26(1):643–696, 1998. doi: https://doi.org/10.1146/annurev.earth.26.1.643.

NCEDC. Northern California Earthquake Data Center. UC Berkeley Seismological Laboratory. *Dataset*, 2014. doi: 10.7932/NCEDC.

Oppenheimer, D. H., Bakun, W. H., and Lindh, A. G. Slip partitioning of the Calaveras Fault, California, and prospects for future earthquakes. *Journal of Geophysical Research: Solid Earth*, 95(B6):8483–8498, 1990. doi: https://doi.org/10.1029/JB095iB06p08483.

Schaff, D. P. and Waldhauser, F. Waveform cross-correlation-

based differential travel-time measurements at the Northern California Seismic Network. *Bulletin of the Seismological Society of America*, 95(6):2446–2461, 2005. doi: https://doi.org/10.1785/0120040221.

Schaff, D. P., Bokelmann, G. H., Beroza, G. C., Waldhauser, F., and Ellsworth, W. L. High-resolution image of Calaveras fault seismicity. *Journal of Geophysical Research: Solid Earth*, 107(B9): ESE–5, 2002. doi: https://doi.org/10.1029/2001JB000633.

Schulz, S. *Catalog of creepmeter measurements in California from 1966 through 1988*. 1989. doi: 10.3133/ofr89650.

Schulz, S. S., Mavko, G. M., Burford, R. O., and Stuart, W. D. Long-term fault creep observations in central California. *Journal of Geophysical Research: Solid Earth*, 87(B8):6977–6982, 1982. doi: https://doi.org/10.1029/JB087iB08p06977.

Segall, P. *Earthquake and volcano deformation*. Princeton University Press, 2010.

Slater, L. and Burford, R. A comparison of long-baseline strain data and fault creep records obtained near Hollister, California. *Tectonophysics*, 52(1-4):481–496, 1979. doi: https://doi.org/10.1016/0040-1951(79)90263-4.

Thurber, C. and Sessions, R. Assessment of creep events as potential earthquake precursors: application to the creeping section of the San Andreas fault, California. *pure and applied geophysics*, 152:685–705, 1998. doi: https://doi.org/10.1007/s000240050172.

Thurber, C. H. Creep events preceding small to moderate earthquakes on the San Andreas fault. *Nature*, 380(6573):425–428, 1996. doi: https://doi.org/10.1038/380425a0.

Trugman, D. T. and Shearer, P. M. GrowClust: A hierarchical clustering algorithm for relative earthquake relocation, with application to the Spanish Springs and Sheldon, Nevada, earthquake sequences. *Seismological Research Letters*, 88(2A):379–391, 2017. doi: https://doi.org/10.1785/0220160188.

Tymofyeyeva, E., Fialko, Y., Jiang, J., Xu, X., Sandwell, D., Bilham, R., Rockwell, T. K., Blanton, C., Burkett, F., Gontz, A., et al. Slow slip event on the Southern San Andreas fault triggered by the 2017 M_w 8.2 Chiapas (Mexico) earthquake. *Journal of Geophysical Research: Solid Earth*, 124(9):9956–9975, 2019. doi: https://doi.org/10.1029/2018JB016765.

Victor, P., Oncken, O., Sobiesiak, M., Kemter, M., Gonzalez, G., and Ziegenhagen, T. Dynamic triggering of shallow slip on forearc faults constrained by monitoring surface displacement with the IPOC Creepmeter Array. *Earth and Planetary Science Letters*, 502:57–73, 2018. doi: https://doi.org/10.1016/j.epsl.2018.08.046.

Wahrhaftig, C., Stine, S. W., and Huber, N. K. Quaternary geologic map of the San Francisco 4 degrees x 6 degrees quadrangle, United States. Technical report, 1993. https://pubs.usgs.gov/publication/i1420(NJ10). Report.

Waldhauser, F. and Schaff, D. P. Large-scale relocation of two decades of Northern California seismicity using cross-correlation and double-difference methods. *Journal of Geophysical Research: Solid Earth*, 113(B8), 2008. doi: 10.1029/2007JB005479.

Zhang, M., Ellsworth, W. L., and Beroza, G. C. Rapid Earthquake Association and Location. *Seismological Research Letters*, 90(6): 2276–2284, 09 2019. doi: 10.1785/0220190052.

Zhu, W. and Beroza, G. C. PhaseNet: a deep-neural-network-based seismic arrival-time picking method. *Geophysical Journal International*, 216(1):261–273, 2019. doi: https://doi.org/10.1093/gji/ggy423.

The article *Microseismicity at the Time of a Large Creep Event*